# Hyperfine structure of $^5I_8 \rightarrow {}^5F_5$ optical transitions within the trigonal center of $CaF_2$:$Ho^{3+}$

Tosporn Boonyarith, John P. D. Martin, and Neil B. Manson
*Laser Physics Centre, Research School of Physical Sciences and Engineering, Australian National University, Canberra, A.C.T. 2601, Australia*
(Received 5 October 1992)

The origin of extra hyperfine lines in two optical transitions in the $^5I_8 \rightarrow {}^5F_5$ region of the trigonal center of $Ho^{3+}$ in $CaF_2$ has been investigated by using optically detected nuclear magnetic resonance and two-laser hole burning. Specific mixing of the excited-state hyperfine wave functions is established by the experimental measurements and, in a theoretical analysis, it is shown that such a mixing can arise from the off-diagonal hyperfine interaction between adjacent $E$ and $A$ states. Normally forbidden transitions gain intensity from the mixing and lead to the appearance of the extra hyperfine lines in the optical spectra. The strengths of the quadrupole, hyperfine, and off-diagonal hyperfine interaction in the ground and excited states are obtained in the analysis.

## I. INTRODUCTION

The optical spectrum associated with the transitions between the ground-state doublet of the $^5I_8$ multiplet and the three lowest energy states of the excited $^5F_5$ multiplet within the trigonal ($C_{3v}$) center of $Ho^{3+}$ in low-doped $CaF_2$:$Ho^{3+}$ samples, also known as the $B$ center,[1] exhibits well-resolved hyperfine structure (Figs. 1 and 2). The nuclear spin of the naturally abundant $^{165}$Ho isotope is $I=7/2$, and the anticipated well-resolved eight line hyperfine patterns are present in these three transitions. In the second and third of these transitions, however, there are extra features that are the focus of attention in this paper. Two high-resolution spectroscopic techniques, namely, optically detected nuclear magnetic resonance (ODNMR) and two-laser hole burning, are used to assist in identifying the origin of the features.

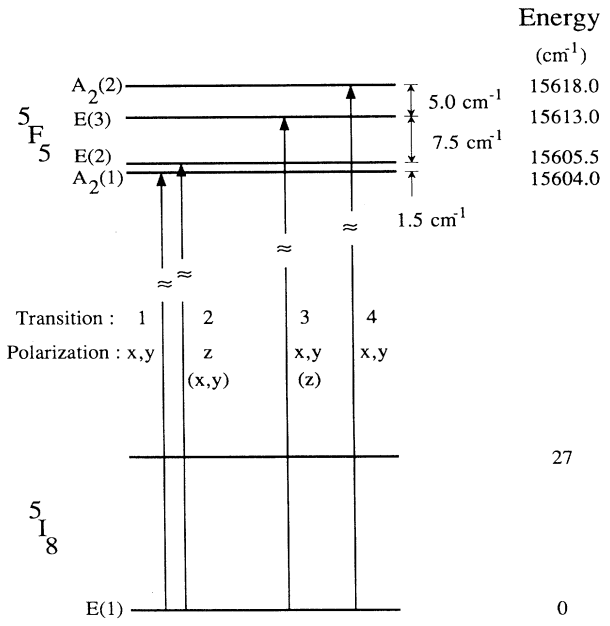


FIG. 1. Energy-level diagram for low-lying levels of the $5I_8$ and $5F_5$ multiplets in the trigonal ($C_{3v}$) center of $Ho^{3+}$ in $CaF_2$.

## II. EXPERIMENTAL DETAILS

The $CaF_2$:$Ho^{3+}$ crystal was grown using the Bridgman technique where a very small quantity of $HoF_3$, $5\times10^{-6}$ mole fraction, was added to the melt. In all of the experiments, the crystal was immersed in a pumped liquid-helium bath. In obtaining the excitation spectrum, the crystal was illuminated by a high-resolution Coherent 699-21 ring dye laser which has a linewidth of 2 MHz. The emitted light was dispersed by a double pass Spex spectrometer (resolution 0.3 nm) and detected by an EMI9958 thermoelectrically cooled photomultiplier.

For the ODNMR experiments, the laser was operated at a fixed frequency corresponding to an hyperfine resolved optical transition and microwaves were applied to the sample held between the plates of a parallel-plate capacitor. A Wavetek 962 MicroSweeper was used and the output was amplified by a Hewlett-Packard 491C microwave amplifier. The changing emission level from the sample was recorded and averaged for repeated sweeps of the microwave frequencies utilizing a Princeton Applied Research 4202 signal averager.

For the two-laser hole burning experiments, a further high-resolution dye laser was incorporated, a Coherent 599-21. One dye laser was tuned to the frequency corresponding to the maximum absorption in one hyperfine line while the excitation of the overall spectrum was mea-

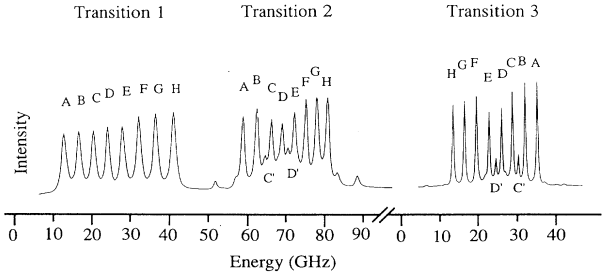


FIG. 2. $^5I_8[E(1)] \rightarrow {}^5F_5[A_2(1),E(2),E(3)]$ excitation spectrum of the trigonal ($C_{3v}$) center of $Ho^{3+}$ in $CaF_2$ at 1.8 K. Transition 3 is six times stronger than transitions 1 and 2.

 

sured as a function of the frequency of the second dye laser.

### III. $^5I_8$ and $^5F_5$ CRYSTAL-FIELD ASSIGNMENTS

The symmetry of the low-lying crystal-field levels of the $^5I_8$ and $^5F_5$ multiplets has been determined from the excitation and emission spectra, and the assignments are summarized in Fig. 1. The observed polarization of the transitions has been used in determining the symmetry of the states although in several cases the identification has been greatly facilitated by the observed hyperfine structure. The resultant assignments are consistent with those made by Mujaji *et al.*[2] on the basis of more precise and more extensive polarized excitation and emission spectra, and in the case of the excited-state singlet levels where our data are insufficient, the specific singlet $A_1$ and $A_2$ assignments of Mujaji *et al.*[2] are accepted.

At helium temperatures, only the lowest level (an $E$ state) of the ground multiplet is populated, therefore, the three lines observed in the $^5I_8 \rightarrow {}^5F_5$ excitation (Fig. 2) are clearly associated with transitions to the three lowest levels of the $^5F_5$ multiplet. The lowest energy optical transition, denoted transition 1, corresponds to an $E \rightarrow A$ transition. Such a transition is only allowed for transverse oscillations $(x,y)$ of the electric-dipole moment, whereas the other two electronic transitions, 2 and 3 (Fig. 2), corresponding to $E \rightarrow E$ transitions are allowed, in principle, by both transverse $(x,y)$ and axial $(z)$ oscillations of the electric-dipole moment. Each polarization can give rise to a set of eight hyperfine lines spaced at either the sum or the difference of the ground- and excited-state hyperfine separations and the intensity of any one set of eight lines will be independent of other sets. In the case of transition 2 (and coincidentally transition 3) it is the closer spaced set of eight hyperfine lines (labeled $A$ to $H$) corresponding to the difference of the ground- and excited-state hyperfine separations that is the stronger set.

Transitions 2 and 3 exhibit different polarization behaviors. In the case of transition 2, the weak sum hyperfine lines are always intensity correlated with the lines in transitions 1 and are $(x,y)$ polarized. The strong hyperfine lines in the case of transition 2 are, therefore, polarized parallel to the trigonal axis $(z)$ and, as these hyperfine lines are separated by the difference in the hyperfine splittings, it can be concluded that (i) the hyperfine levels in the initial and final state are in the same order and (ii) the $Ho^{3+}$ magnetic moment has the same sign in the ground state and the second excited state of the $^5F_5$ multiplet. The reversed situation in transition 3 means that the third excited state of the $^5F_5$ multiplet has a $g$ value of the opposite sign to that of the ground state and the second excited state.

In the above brief analysis it is taken that the optical pattern is composed of two sets of eight hyperfine lines, one strong and one weak. This is not entirely correct as in both the cases of transitions 2 and 3 there are two extra lines of intermediate intensity within the spectrum (Fig. 2). With the reversal of the polarization behaviors, it is convenient to also reverse the labeling of the order of the eight hyperfine lines $A$ to $H$ making the extra lines in both transitions lie between $B$ and $C$ (denoted $C'$) and between $D$ and $E$ (denoted $D'$). It is these features that have an unusual origin and accounting for their presence is the primary concern of this paper. The structure in transition 3 was reported by Hasan *et al.*[3] but no analysis of the structure was given.

There is a fourth low-lying level in the $^5F_5$ multiplet. The optical transition to this level also exhibits hyperfine structure, but with larger linewidth and much lower intensity (not shown). Polarization data and crystal-field analysis[2] indicate that the level is a singlet of $A_2$ symmetry. As the theoretical analysis presented below involves this level, it is shown on the energy-level diagram in Fig. 1.

Another curious feature of the $^5I_8 \rightarrow {}^5F_5$ excitation spectrum is that transition 3 exhibits the narrowest hyperfine lines with a linewidth of $\sim 1$ GHz, even though the transition is to the third state in the excited $^5F_5$ multiplet. The reason for this alternative situation here is not investigated in detail but clearly the nature of the wave functions associated with transition 3 must result in it being less susceptible to frequency shifts arising from random internal crystal stresses or there is slow relaxation between this state and the two lower ones.[4]

### IV. GROUND-STATE ODNMR RESULTS

The observed ground-state hyperfine ODNMR spectrum is shown in Fig. 3. The spectrum is dependent on the hyperfine level resonant with the laser, but not on which of the three optical transitions is excited. When the laser is tuned to either of the extreme hyperfine lines ($A$ or $H$), two ODNMR signals are observed at 3.816 and 3.897 GHz [Fig. 3(a)]. When the laser is tuned to the next lowest or highest hyperfine line ($B$ or $G$), four

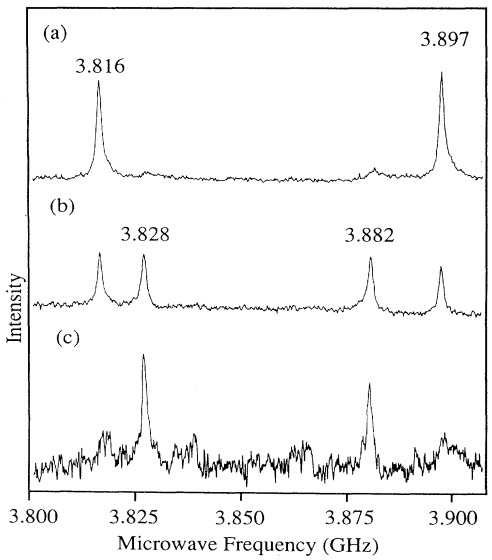


FIG. 3. ODNMR spectrum for $Ho^{3+}$ in $CaF_2$. Traces (a), (b), and (c) correspond to hole burning in hyperfine lines $A$, $B$, and $C$ of the third electronic transition, respectively.

ODNMR signals are observed at 3.816, 3.828, 3.882, and 3.897 GHz [Fig. 3(b)]. Subsequent lines give less clear spectra with some of the same frequencies reoccurring [Fig. 3(c)]. Central lines at 3.867 and 3.840 GHz have been observed but with less accuracy.

## V. HYPERFINE STRUCTURE OF THE $^5I_8$ GROUND MULTIPLET

The Hamiltonian that describes the hyperfine interaction is given by

$$\begin{aligned}\mathcal{H}_{\text{hyperfine}} &= \mathcal{H}_M + \mathcal{H}_Q + \mathcal{H}_{Q'} \\ &= \hbar\{[A_{\parallel} I_z J_z + \tfrac{1}{2} A_{\perp}(I_+ J_- + I_- J_+)] \\ &\quad + P_{4f}[2(\mathbf{J}\cdot\mathbf{I})^2 + \mathbf{J}\cdot\mathbf{I} - \tfrac{2}{3}J(J+1)I(I+1)] \\ &\quad + P_{\text{latt}}[I_z^2 - \tfrac{1}{3}I(I+1)]\} , \end{aligned} \tag{1}$$

where (i) $\mathcal{H}_M(\mathcal{H}_Q)$ are the dipole (quadrupole) hyperfine interactions between the holmium nucleus and its host ions,[5] and (ii) $\mathcal{H}_{Q'}$ is the interaction of the holmium nucleus with the electric-field gradient produced by the neighboring ions. The dipole hyperfine interaction parameter is $\sim 4-5$ GHz for the ground state, this being much smaller than the separation of 27 $cm^{-1}$ (800 GHz) to the nearest state. The direct quadrupole interaction parameters are smaller again $\sim 0-50$ MHz and as such $\mathcal{H}_Q$ is usually approximated to first order as $P_{4f}\langle 3J_z^2 - J(J+1)\rangle[I_z^2 - I(I+1)/3]$. The ground $E$ level can therefore be considered as an isolated state with the effect of the hyperfine interactions giving only small quadrupole shifts. In fitting the hyperfine separations, the pseudoquadrupole term arising from the dipole hyperfine interaction admixing higher states can be treated by adjusting the value of the effective total quadrupole interaction parameter $P$. The hyperfine separations themselves are dominated by the diagonal terms in the Hamiltonian and can be accurately determined by optical microwave double-resonance experiments.

With the laser frequency coincident with a hyperfine transition, a subgroup of $Ho^{3+}$ ions is excited from a ground-state hyperfine level to an excited-state hyperfine level. Reorientation of the nuclear spin can occur before the excited center returns to the ground state. When this occurs, the $Ho^{3+}$ ions will no longer be resonant with the laser, thus producing a spectral hole. Irradiation at microwave frequencies corresponding to the separations between the hyperfine levels, however, can restore the ions to their original ground-state hyperfine level and reestablish resonance with the laser. This situation will be registered as an increase in absorption and subsequent emission. The response is termed, due to the analogous rf experimental technique, as an ODNMR signal.

It is only microwave transitions between adjacent hyperfine sublevels that are allowed in first order and when hole burning in the extreme line $A$, the lowest hyperfine level ($I_z = \pm 7/2$) should only be repopulated when the transition with the adjacent level ($I_z = \pm 5/2$) is excited. Hence, for the laser resonant with the line $A$, the ODNMR technique gives a signal at 3.816 GHz. However, a second line at 3.897 GHz is also observed and it arises because there is a fast reorientation of the electron spin in the ground-state doublet between the two electronic components having the same nuclear projection. A similar effect has been observed in the ODNMR spectrum of $LaCl_3$:$Ho^{3+}$ (Ref. 6). Hence, with the laser resonant with either of the extreme hyperfine lines ($A$ or $H$), two ODNMR signals at 3.816 and 3.897 GHz are observed.

With the laser resonant with the second lowest hyperfine transition, the $I_z = \pm 5/2$ levels in the ground state are depopulated and the population can be restored via transitions from the two adjacent hyperfine levels $I_z = \pm 3/2$ and $I_z = \pm 7/2$. Hence, the frequency corresponding to the separation between the two lowest hyperfine levels occurs, plus the frequency corresponding to that between the second and third hyperfine levels. With significant electron spin flipping occurring, the frequencies for the two separations between the three highest sublevels of the $E$ state are also present. Thus, when hole burning in either the $B$ or $G$ hyperfine transitions, there are four resonances observed at 3.816, 3.828, 3.882, and 3.897 GHz. The progression is expected to be repeated for the other hyperfine lines, and this is partially true. However, for levels nearer the center of the hyperfine pattern, population storage through a change in the nuclear-spin projection directly competes with the electron spin-flip process and, in addition, these inner levels are more susceptible to inhomogeneous broadening.

TABLE I. Energy separations between hyperfine levels of the ground state $^5I_8[E(1)]$ as obtained from the ODNMR experiments.

| Crystal-field level (energy, $cm^{-1}$) | Hyperfine transitions[a] | Experimental hyperfine splittings (GHz) | Calculated hyperfine splittings (GHz) with $A'_{\parallel} = -3.855 \pm 0.003$ GHz $P = 6.8 \pm 0.5$ MHz |
|---|---|---|---|
| $^5I_8[E(1)]$ | $\mp 7/2 \leftrightarrow \mp 5/2$ | $3.897 \pm 0.003$ | $3.896 \pm 0.004$ |
| (0) | $\mp 5/2 \leftrightarrow \mp 3/2$ | $3.882 \pm 0.003$ | $3.882 \pm 0.004$ |
| | $\mp 3/2 \leftrightarrow \mp 1/2$ | $3.867 \pm 0.005$ | $3.869 \pm 0.003$ |
| | $\mp 1/2 \leftrightarrow \pm 1/12$ | | $3.855 \pm 0.003$ |
| | $\pm 1/2 \leftrightarrow \pm 3/2$ | $3.840 \pm 0.005$ | $3.842 \pm 0.003$ |
| | $\pm 3/2 \leftrightarrow \pm 5/2$ | $3.828 \pm 0.003$ | $3.828 \pm 0.004$ |
| | $\pm 5/2 \leftrightarrow \pm 7/2$ | $3.816 \pm 0.003$ | $3.815 \pm 0.004$ |

[a]The upper signs are for $|E_+\rangle$ whereas the lower signs are for $|E_-\rangle$.

As a result of these effects, the additional hyperfine resonances do not give clear features in the ODNMR spectrum [Fig. 3(c)]. Similar observation of strong ODNMR signals when pumping extreme hyperfine lines and poor signals when pumping central lines has been noted before in another system.[6]

From the above analysis it can be seen that the frequencies obtained from the ODNMR measurements give a very accurate measurement of the splitting of the hyperfine levels in the $^5I_8$ ground state and these are listed in Table I. From the experiment, the strength of the interactions is readily determined. For example, the effective axial dipole hyperfine coupling constant in the ground-state doublet

$$A'_{\parallel} = A_{\parallel}(^5I_8)\langle J_z \rangle \tag{2}$$

is found to be $-3.855(3)$ GHz, where $A_{\parallel}(^5I_8)$ is the intrinsic axial dipole hyperfine coupling constant for the $C_{3v}$ center of $^{165}$Ho:$CaF_2$ in the $^5I_8$ multiplet, and $\langle J_z \rangle$ is the expectation value of the $z$ component of the electronic spin of the ground doublet state. The effective quadrupole splitting strength (electric quadrupole plus pseudoquadrupole) is found to be $+6.8(5)$ MHz.

## VI. HYPERFINE STRUCTURE OF THE $^5F_5$ STATES

### A. Lowest level $^5F_5(A)$

As seen in Fig. 2, transition 1 has a simple eight line pattern as expected for an $A \rightarrow E$ transition and, since the ground-state splittings are known from the above ODNMR analysis, the excited-state separations are easily deduced from the optical separations. The excited-state splittings are listed in Table II. The values rely on the measurement of separation of the inhomogeneously broadened optical lines and consequently the accuracy is poorer than that obtained for the ground state using direct microwave measurements.

For singlet states, the admixture of other states via the dipole hyperfine interaction gives rise to pseudoquadrupole shifts of the hyperfine levels of the same form as

TABLE II. Energy separations between hyperfine levels of the four lowest crystal-field states [$A_2(1)$,$E(2)$,$E(3)$, and $A_2(2)$] in the excited $^5F_5$ multiplet.

| Crystal-field level (energy, $cm^{-1}$) | Hyperfine transitions[a] | Experimental hyperfine splittings[b] (GHz) | Calculated hyperfine splittings (GHz) |
|---|---|---|---|
| $^5F_5[A_2(2)]$ | $\pm1/2 \leftrightarrow \pm3/2$ | | 0.129[e] |
| (15 618.0) | $\pm3/2 \leftrightarrow \pm5/2$ | | 0.258[e] |
| | $\pm5/2 \leftrightarrow \pm7/2$ | | 0.389[e] |
| $^5F_5[E(3)]$ | $\pm7/2 \leftrightarrow \pm5/2$ | 0.97±0.03 | 1.235[e] |
| (15 613.0) | $\pm5/2 \leftrightarrow \pm3/2$ | 0.92±0.03 | 1.145[e] |
| | $\pm3/2 \leftrightarrow \pm1/2$ | 0.89±0.03 | 1.049[e] |
| | $\pm1/2 \leftrightarrow \mp1/2$ | 0.83±0.03 | 0.878[e] |
| | $\mp1/2 \leftrightarrow \mp3/2$ | 1.40±0.03 | 1.396[e] |
| | | [1.39±0.03][c] | |
| | $\mp3/2 \leftrightarrow \mp5/2$ | 0.70±0.03 | 0.749[e] |
| | $\mp5/2 \leftrightarrow \mp7/2$ | 0.85±0.03 | 0.791[e] |
| $^5F_5[E(2)]$ | $\mp7/2 \leftrightarrow \mp5/2$ | 0.62±0.03 | 0.713[f] |
| (15 605.5) | $\mp5/2 \leftrightarrow \mp3/2$ | 0.55±0.03 | 0.642[f] |
| | $\mp3/2 \leftrightarrow \mp1/2$ | 1.45±0.03 | 1.612[f] |
| | | [1.37±0.03][d] | |
| | $\mp1/2 \leftrightarrow \pm1/2$ | 1.04±0.03 | 0.802[f] |
| | $\pm1/2 \leftrightarrow \pm3/2$ | 0.91±0.03 | 1.038[f] |
| | $\pm3/2 \leftrightarrow \pm5/2$ | 1.03±0.03 | 1.182[f] |
| | $\pm5/2 \leftrightarrow \pm7/2$ | 1.31±0.03 | 1.326[f] |
| $^5F_5[A_2(1)]$ | $\pm7/2 \leftrightarrow \pm5/2$ | 0.50±0.03 | 0.512[f] |
| (15 604.0) | $\pm5/2 \leftrightarrow \pm3/2$ | 0.34±0.03 | 0.335[f] |
| | $\pm3/2 \leftrightarrow \pm1/2$ | 0.15±0.03 | 0.189[f] |

[a]For the doublet states, the upper and lower signs are for $|E_+\rangle$ and $|E_-\rangle$, respectively.
[b]Calculated from the difference between optical and ODNMR spectra.
[c]Measured directly from optical spectrum.
[d]Measured directly from optical spectrum. However, in this case, the presence of the weak allowed transverse polarized lines and the large linewidths (Fig. 2) makes it more difficult to determine the exact positions of the extra lines.
[e]Obtained by treating the $^5F_5[A_2(2)]$ and $^5F_5[E(3)]$ levels as an isolated system with $A'_{\parallel}=1$ GHz and $|A'_{\perp}|=4.45$ GHz.
[f]Obtained by treating the $^5F_5[E(2)]$ and $^5F_5[A_2(1)]$ levels as an isolated system with $A'_{\parallel}=-1$ GHz and $|A'_{\perp}|=2.82$ GHz.

those arising from the electric quadrupole interaction. Hence, the hyperfine levels of the excited-state singlet can be fitted to a single effective quadrupole splitting factor of $P=0.08(2)$ MHz. The individual contributions to the splittings cannot currently be separated using the zero-field experimental data, but the analysis given below suggests that these splittings arise predominantly from the coupling with the adjacent $E$ state.

### B. Doublet states $^5F_5(E)$

The expected pattern for an $E \rightarrow E$ transition includes lines at the sum and the difference of hyperfine separations, and the majority of lines within the optical transitions 2 and 3 can be accounted for in this way. Furthermore, with knowledge of the ground-state splittings, the optical frequencies can be used to determine the separations of the hyperfine levels in the excited $E$ state, and they are listed in Table II. It can be seen that there are irregularities in the spacing of the hyperfine levels and, in particular, there is a larger gap between two of the central levels. The origin for this larger splitting is the subject of the subsequent discussion in this paper, and it will be shown that the extra lines $C'$ and $D'$ involve the states with the larger splitting.

## VII. TWO-LASER HOLE BURNING SPECTRA

The observed two-laser hole burning spectra for transition 3 are shown in Fig. 4. With one laser tuned to a single hyperfine line, the hole burning spectrum measured by the other laser gives a spectrum dominated by a hole on the resonant hyperfine line. In addition to this main hole, electron-spin flips give a hole in the other doublet component with the same nuclear spin projection. There is also loss of nuclear-spin memory during the optical cycle giving holes/antiholes on other hyperfine lines.[6,7] These occurrences tally with the ability to observe ODNMR signals; however, the size of these additional holes are small and hardly discernible in Fig. 4.

There is, however, a new feature observed in the hole burning spectrum of the $B$ center that is distinct from that previously reported for $E \rightarrow E$ transitions. When the laser is used to saturate the absorption (burn a hole) at the extra hyperfine line $C'$ (or $D'$), a hole of significant relative size is also observed on the adjacent strong hyperfine line $C(D)$, and vice versa (Fig. 4). This leads to the conclusion that the hyperfine lines $C$ and $C'$ (also $D$ and $D'$) originate from the same ground-state hyperfine level. To support this assignment, the separations between hyperfine lines $C$ and $C'$ and between $D$ and $D'$ must correspond to the separations between the associated hyperfine levels in the excited state. For optical transition 3, the separations of $C$-$C'$ and $D$-$D'$ are both 1.39(3) GHz consistent with the excited-state separation given in Table II determined from the optical and microwave data. The value corresponds to the largest gap between adjacent excited-state hyperfine levels, and is, from the position in the hyperfine spectrum, associated either with the separation between $|E_{\pm}, \mp 1/2\rangle$ and $|E_{\pm}, \mp 3/2\rangle$, or between $|E_{\mp}, \pm 1/2\rangle$ and $|E_{\pm}, \mp 3/2\rangle$.

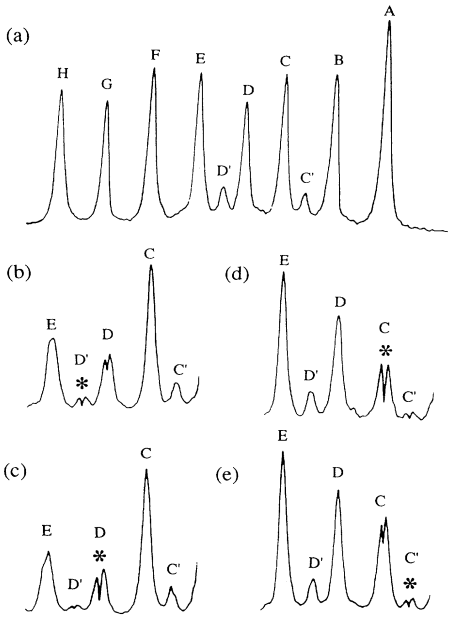


FIG. 4. Two laser optical hole burning. (a) The unburned spectrum of the optical transition 3. (b)–(e) The hole burning spectra associated with hole burning in the hyperfine lines $D', D, C$, and $C'$, respectively. The asterisks are used to indicate the frequency of the burn laser.

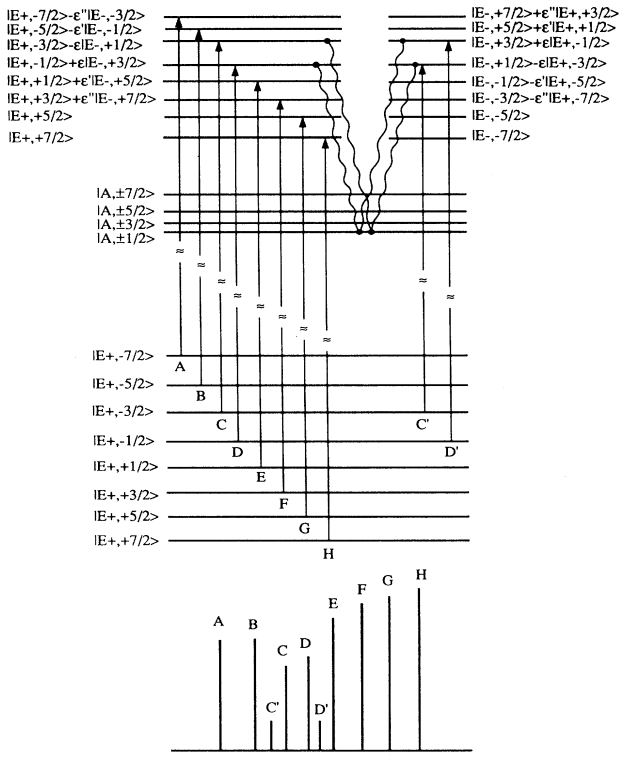


FIG. 5. Illustration of origin of hyperfine induced transitions. The solid vertical lines indicate the transitions whereas the irregular lines indicate the states coupled by the transverse dipole hyperfine interaction. The coupling mechanisms are only shown for two pairs of the doublet hyperfine levels; four other pairs are similarly coupled as discussed in the text.

Here the basis states are of the form $|\Gamma, I_z\rangle$, where $\Gamma$ and $I_z$ denote the $z$ component of the electronic and nuclear spins, respectively. Allowing for the reversal of the ordering of the hyperfine lines, the hole burning behavior is the same for transition 2.

From the above, it can be concluded that the extra lines arise from transitions from a ground-state hyperfine level with a particular nuclear spin projection to an excited state with a different nominal spin projection. In the particular case of transition 2, it will be shown that (Fig. 5) the regular hyperfine line $C$ is associated with transitions from the ground $|E_{\pm}, \mp 3/2\rangle$ states to the excited $|E_{\pm}, \mp 3/2\rangle$ states (i.e., $|E_+, -3/2\rangle \rightarrow |E_+, -3/2\rangle$ and $|E_- +3/2\rangle \rightarrow |E_-, +3/2\rangle$), whereas the extra line $C'$ is between the same ground states and the excited states with nominal designation $|E_{\mp}, \pm 1/2\rangle$. In fact, the observation of the extra lines implies that a mixing has occurred and that one or both of the states with nominal designation $|E_{\mp}, \pm 1/2\rangle$ has a significant $|E_{\pm}, \mp 3/2\rangle$ component. This mixing is indicated in Fig. 5 and its origin is discussed in the following section.

## VIII. MIXING BETWEEN THE HYPERFINE LEVELS OF AN $E$ AND AN $A$ STATE BY THE DIPOLE HYPERFINE INTERACTION

The lower levels of the $^5F_5$ multiplet comprises two singlet $A_2$ states and two doublet $E$ states, all within a few wave numbers (Fig. 1). The above analysis of the two-laser hole burning has shown that a specific type of mixing has occurred, and the distinct character of this mixing is that only two out of the eight hyperfine levels have been significantly affected. By considering the effect of the hyperfine interaction, it is found that the admixture of nearby doublet states affects all 16 hyperfine functions of an $E$ state by a similar amount. This even mixing mechanism can therefore be dismissed as the origin of the two extra hyperfine transitions. The coupling between an $E$ and $A$ state, however, does give asymmetric mixing of the wave functions and will be discussed below.

The effect of the dipole hyperfine interaction on the $E$ and $A$ ($A_1$ or $A_2$) states separated by an energy $D$ is considered. It is assumed that there is no interaction with any other state and that there is no quadrupole interaction. The axial component of the dipole hyperfine interaction, $A_{\parallel} I_z J_z$, gives rise to the dominant hyperfine splitting of the $E$ state. The transverse dipole hyperfine interaction, $A_{\perp}(I_+ J_- + I_- J_+)/2$, is the term that causes the admixture of the hyperfine components of the $E$ and $A$ electronic states.

Each hyperfine state $|A, I_z\rangle$ (except $|A, \pm 7/2\rangle$) associated with the electronic singlet interacts with a pair of the doublet hyperfine states $|E_+, I_z - 1\rangle$ and $|E_-, I_z + 1\rangle$ and the resultant energies are obtained by diagonalizing the Hamiltonian matrix,

$$\begin{pmatrix} D+(I_z-1)A'_{\parallel} & \frac{1}{2}A'_{\perp}\sqrt{(I+I_z)(I-I_z+1)} & 0 \\ \frac{1}{2}A'_{\perp}\sqrt{(I+I_z)(I-I_z+1)} & 0 & \frac{1}{2}A''_{\perp}\sqrt{(I-I_z)(I+I_z+1)} \\ 0 & \frac{1}{2}A''_{\perp}\sqrt{(I-I_z)(I+I_z+1)} & D-(I_z+1)A'_{\parallel} \end{pmatrix} \tag{3}$$

where the matrix elements multiplied by the dipole hyperfine interaction parameters have been rewritten as effective dipole hyperfine interaction strengths $A'_{\parallel}$, $A'_{\perp}$, and $A''_{\perp}$ defined by

$$A'_{\parallel} = A_{\parallel}\langle E_+ | J_z | E_+ \rangle = -A_{\parallel}\langle E_- | J_z | E_- \rangle \ , \tag{4}$$

$$A'_{\perp} = A_{\perp}\langle E_+ | J_+ | A \rangle = A_{\perp}\langle A\, J_- | E_+ \rangle \ , \tag{5}$$

and

$$A''_{\perp} = A_{\perp}\langle E_- | J_- | A \rangle = A_{\perp}\langle A | J_+ | E_- \rangle \ . \tag{6}$$

In the case of the crystal field of $C_{3v}$ symmetry, an $A_2$ singlet has the property that $A'_{\perp} = A''_{\perp}$, whereas for an $A_1$ singlet $A'_{\perp} = -A''_{\perp}$.

By using perturbation theory on the above matrix,[8] two types of correction terms to the energies arise. The first type has denominators of the form $D^n$ where $D$ is the separation between the doublet and singlet, and $n$ is an integer. The leading term of this type is the familiar pseudoquadrupole contribution which is proportional to $(A'_{\perp})^2/D$. The second term of this type is $\sim A'_{\parallel}(A'_{\perp})^2/D^2$ which, for $A_{\parallel} = 1$ GHz and $D = 45$ GHz, is at most only a few percent of the pseudoquadrupole strength.

The second type of correction terms has denominators of the form $A''^{m}_{\parallel} D^{2n}$ where $m$ and $n$ are integers. Importantly, these terms describe the repulsion between the two $E$-state hyperfine levels. The leading term of this type arises in fourth order and is $\sim (A'_{\perp})^4/A'_{\parallel} D^2$. It will be shown that when $A'_{\perp}$ is larger than $A'_{\parallel}$ this term can become more significant than the pseudoquadrupole contribution and quantitatively describes the observed mixing among the $E$-state hyperfine levels.

From the form of the Hamiltonian matrix (3), the wave functions for the doublet hyperfine states take the form

$$|E_+, I_z - 1\rangle = |E_+, I_z - 1\rangle + \delta |A, I_z\rangle + \varepsilon |E_-, I_z + 1\rangle \ , \tag{7}$$

where $\delta$, the normal pseudoquadrupole correction, is

$$\delta \equiv \tfrac{1}{2}\sqrt{(I+I_z)(I-I_z+1)}\,\frac{A'_{\perp}}{D} \tag{8}$$

and the extra correction term is

$$\varepsilon \equiv \frac{\sqrt{(I+I_z)(I-I_z+1)(I-I_z)(I+I_z+1)}}{8I_z}\,\frac{A'_{\perp}A''_{\perp}}{A'_{\parallel}D} \ . \tag{9}$$

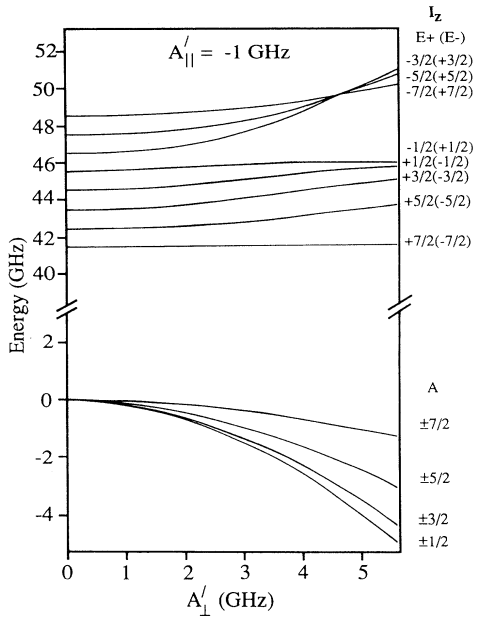


FIG. 6. Energy-level diagram of an $E$ and an $A$ state separated by 45 GHz and coupled by the transverse dipole hyperfine interaction.

As can be seen in Eq. (9), the expression for $\varepsilon$ contains the energy denominator, $2I_z A'_{\parallel}$, which is the separation between the coupled hyperfine levels in the $E$ state. Three pairs of $E$-state hyperfine levels (and their complex conjugates) exhibit the above form of coupling, and the respective mixing coefficients are

(i) $|E_{\pm}, \mp 1/2\rangle$ and $|E_{\mp}, \pm 3/2\rangle$:

$$\varepsilon = \pm\sqrt{15}\frac{A'_{\perp}A''_{\perp}}{A'_{\parallel}D} , \tag{10}$$

(ii) $|E_{\pm}, \pm 1/2\rangle$ and $|E_{\mp}, \pm 5/2\rangle$:

$$\varepsilon' = \pm\frac{\sqrt{5}}{2}\frac{A'_{\perp}A''_{\perp}}{A'_{\parallel}D} , \tag{11}$$

(iii) $|E_{\pm}, \pm 3/2\rangle$ and $|E_{\mp}, \pm 7/2\rangle$:

$$\varepsilon'' = \pm\frac{\sqrt{21}}{10}\frac{A'_{\perp}A''_{\perp}}{A'_{\parallel}D} . \tag{12}$$

The mixing is largest in case (i) where adjacent states are coupled, and the presence of mixed states results in extra transitions of intensity $\varepsilon^2$ in first order (where regular hyperfine lines are defined to have unit intensity). The coupling and the extra transitions $C'$ and $D'$ caused by the mixing in case (i) are indicated in Fig. 5 for transition 2 where the $g$ values of the ground- and the excited-state doublets have the same sign and the $z$ polarized optical transition is strongest. Extra transitions will also be present in the $x,y$ polarized spectrum but, for clarity, this polarization is not included. The mixing in the cases of (ii) and (iii) gives similar effects but the magnitudes are smaller and hence the extra lines induced will be substantially weaker (to avoid complexity these are also omitted in Fig. 5). In principle, the admixture of the $A$ hyperfine states into the $E$ hyperfine states, described by the pseudoquadrupole term $\delta$ and weaker corrections, gives rise to extra $(4I\text{-}1)$ transverse polarized lines in the $E \rightarrow E$ transition. However, the mixing coefficients $\delta$ are typically an order of magnitude weaker than $\varepsilon$, and so the resultant extra lines will be correspondingly small.

In Fig. 6, the effect of the transverse part of the dipole hyperfine interaction on the hyperfine levels of a pair of coupled singlet and doublet states is more fully illustrated. Because the repulsion between the $E$-state hyperfine levels arises from high-order perturbation terms, the energy levels shown in Fig. 6 have been obtained from a full numerical diagonalization of the Hamiltonian matrix (3). This diagram shows, for example, that the energy separation between the $|E_{\pm}, \mp 1/2\rangle$ and $|E_{\pm}, \mp 3/2\rangle$ hyperfine levels is most susceptible to the strength of the transverse dipole hyperfine interaction, and it is this separation for which a change in the regular spacing of the hyperfine lines will be most noticeable. In particular, as soon as $A'_{\perp}$ is larger than $A'_{\parallel}$, the energy shifts become significant compared with the hyperfine splitting. The figure also shows that even more unusual splittings are possible

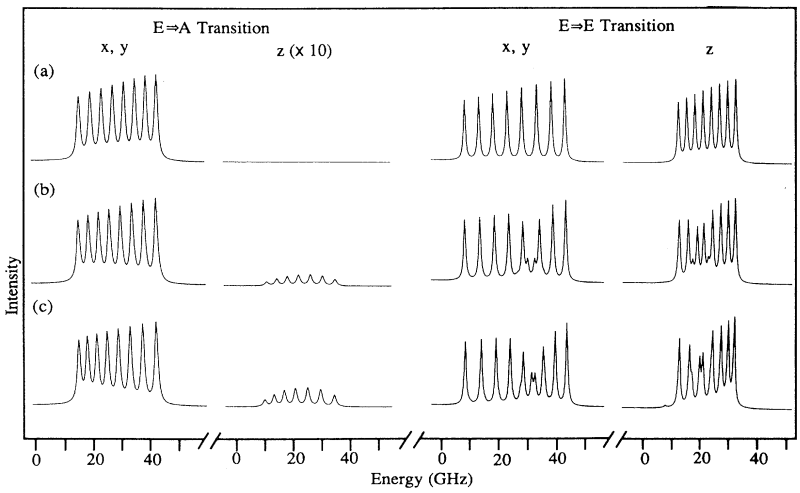


FIG. 7. Intensity pattern predicted for transitions from an isolated ground-state doublet with $A'_{\parallel} = -3.855$ GHz to excited states comprising of an $A$ and an $E$ state separated by 45 GHz and coupled by the transverse dipole hyperfine interaction. For the excited state, $A'_{\parallel} = -1$ GHz, and three different values of $A'_{\perp}$ have been used to demonstrate the changing of the intensity pattern; (a) $A'_{\perp} = 0$ GHz, (b) $A'_{\perp} = 2.82$ GHz, and (c) $A'_{\perp} = 4.45$ GHz. The transition strengths are weighted by the intensity ratios

$$\mathcal{I}_z(E \rightarrow E) : \mathcal{I}_{x,y}(E \rightarrow E) : \mathcal{I}_{x,y}(E \rightarrow A) = 1:1:1 .$$

when $A'_\perp$ is large compared to $A'_\parallel$. The hyperfine splittings within the $A$ electronic state, on the other hand, are always a reasonable approximation to that expected for a quadrupole effect (Fig. 6).

In addition to the hyperfine splittings, the relative transition intensities can be fitted with knowledge of the eigenstates. Figure 7 displays the expected optical spectra for $A'_\perp = 0$, 2.82, and 4.45 GHz. For the middle value, the situation approaches that described in the perturbation treatment discussed above where only two significant extra lines are induced into the optical spectrum towards the center of the hyperfine pattern. As can be seen, the intensity of the extra lines is at the cost of strength of adjacent lines. When the extra lines have comparable intensity to the regular hyperfine lines, as occurs for the largest value of $A'_\perp = 4.45$ GHz, the variation from equal spacing becomes apparent and further weak transitions can be observed. These are illustrated for the $z$ and $x,y$ polarized transitions (Fig. 7).

In the above treatment, it was assumed that the $E$ state only interacted with a single $A$ state. Clearly, if other states in the multiplet are also mixed into the $E$ state, the situation will change and is likely be more complex. The effect of other $A$ states of the same symmetry can be anticipated. Each can give rise to pseudoquadrupole and higher-order shifts (terms $\sim 1/D^n$) but if the $A$ states lie on opposite sides of the $E$ state these shifts can partially cancel. On the other hand, the terms $\sim 1/(A'^{\,m}_\parallel D^{2n})$ will only add constructively such that the mixing within the $E$-state hyperfine levels will increase.

## IX. COMPARISON WITH EXPERIMENT

The two lowest levels of the $5F_5$ multiplet are an $A_2$ and an $E$ state separated by only 1.5 $cm^{-1}$, and they are separated from other states by 7.5 $cm^{-1}$ (Fig. 1). Given the proximity of the levels, it is highly possible that the transverse dipole hyperfine interaction is significant, and that the effect of other states is small. If this is the case then the anticipated optical spectrum will correspond to the calculation of the simple model presented in the previous section and the axial dipole hyperfine interaction, the transverse dipole hyperfine interaction, and the ratio of $z$ to $(x,y)$ polarized transitions can be chosen to give the best correspondence with the optical spectrum.

With $A'_\parallel = -1.0$ GHz, $|A'_\perp| = 2.82$ GHz and intensity ratio

$$\mathscr{I}_z(E \rightarrow E):\mathscr{I}_{x,y}(E \rightarrow E):\mathscr{I}_{x,y}(E \rightarrow A) = 10:1.5:8 \ , \qquad (13)$$

the calculated spectrum is given in Fig. 8. It is noted that very good agreement is obtained with the experimental trace for transitions 1 and 2 shown in Fig. 2. The energy separation between hyperfine levels calculated with the above strengths of the effective hyperfine interaction are listed in Table II. It is seen that, with this model, there is general agreement between experiment and theory, and the disparity is readily attributable to the simplicity of the model with the neglect of the quadrupole hyperfine interactions and the presence of other states.

The second lowest $E$ state in the $^5F_5$ multiplet has an electronic singlet state located 5 $cm^{-1}$ to higher energy.

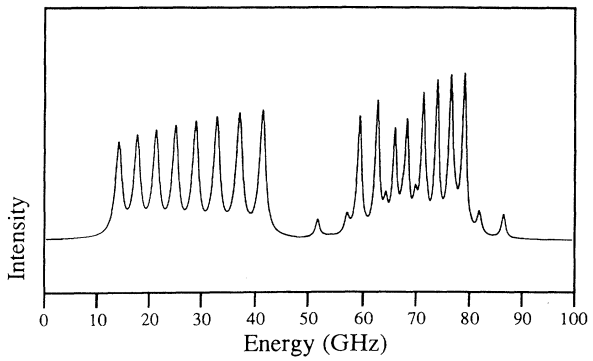


FIG. 8. Intensity pattern predicted for $E \rightarrow A,E$ transitions with the excited states separated by 45 GHz and coupled by the dipole hyperfine interaction. In the ground state $A'_\parallel = -3.855$ GHz whereas in the excited state $A'_\parallel = -1$ GHz and $A'_\perp = 2.825$ GHz. The transition strengths are weighted by the intensity ratios

$$\mathscr{I}_z(E \rightarrow E):\mathscr{I}_{x,y}(E \rightarrow E):\mathscr{I}_{x,y}(E \rightarrow A) = 10:1.5:8 \ .$$

This pair of levels, likewise, is treated in isolation and with $A'_\parallel = +1.0$ GHz, $|A'_\perp| = 4.45$ GHz, and intensity ratio

$$\mathscr{I}_z(E \rightarrow E):\mathscr{I}_{x,y}(E \rightarrow E):\mathscr{I}_{x,y}(E \rightarrow A) = 0.25:10:0 \qquad (14)$$

gives the calculated $E \rightarrow E$ spectrum shown in Fig. 9. This spectrum makes a reasonable comparison with the structure for transition 3 as shown in Fig. 2. Again, there is general agreement between experiment and theory for the values of the hyperfine separations (Table II), and the disparities are attributed to the simplicity of the model.

It is clear that the extra features that occur within the regular hyperfine structure of the two $^5I_8(E) \rightarrow {}^5F_5(E)$ transitions result as a consequence of the excited $E$ states interacting with their neighboring electronic singlet states. However, being able to obtain a reasonable agreement between experiment and calculation by simply al-

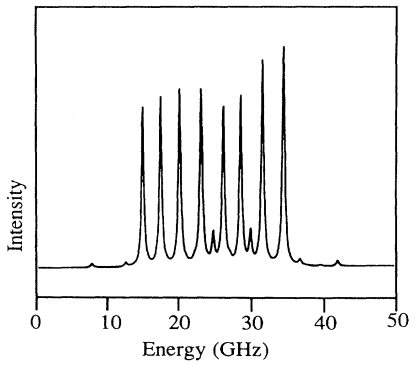


FIG. 9. Intensity pattern predicted for an $E \rightarrow E$ transition with the excited $E$ state coupled to higher energy $A$ state (150 GHz). In the ground state $A'_\parallel = -3.855$ GHz whereas in the excited state $A'_\parallel = 1$ GHz and $A'_\perp = 4.45$ GHz. The transition strengths are weighted with intensity ratio

$$\mathscr{I}_x(E \rightarrow E):\mathscr{I}_{x,y}(E \rightarrow E):\mathscr{I}_{x,y}(E \rightarrow A) = 0.25:10:0 \ .$$

TABLE III. Calculated effective hyperfine interaction strengths. The matrix elements for the $J_z$, $J_+$, and $J_-$ operators between the four lowest crystal-field states in the $^5F_5$ multiplet [$A_2(1), E(2), E(3)$, and $A_2(2)$] are calculated from the crystal-field wave functions of Mujaji *et al.* (Ref. 2). Values in parentheses give values of effective hyperfine interaction strengths used in the calculation of the optical spectrum. Values in square brackets give values of crystal-field energies relative to that of the lowest crystal-field level, $A_2(1)$.

| $^5F_5$ | $A_2(1)$ | $E_+(2)$ | $E_-(2)$ | $E_+(3)$ | $E_-(3)$ | $A_2(2)$ |
|---|---|---|---|---|---|---|
| $A_2(1)$ | 0 [0 GHz] | $4.23A_\perp$ (2.82) | $4.23A_\perp$ (2.82) | $1.46A_\perp$ | $1.46A_\perp$ | 0 |
| $E_+(2)$ | $4.23A_\perp$ (2.82) | $-1.36A_\parallel$ $(-1)$ [45 GHz] | 0 | $0.76A_\parallel$ | $-4.79A_\perp$ | $-0.47A_\perp$ |
| $E_-(2)$ | $4.23A_\perp$ (2.82) | 0 | $1.36A_\parallel$ (1) [45 GHz] | $4.79A_\perp$ | $-0.76A_\parallel$ | $-0.47A_\perp$ |
| $E_+(3)$ | $1.46A_\perp$ | $0.76A_\parallel$ | $4.79A_\perp$ | $0.96A_\parallel$ (1) [270 GHz] | 0 | $5.01A_\perp$ (4.45) |
| $E_-(3)$ | $1.46A_\perp$ | $-4.79A_\perp$ | $-0.76A_\parallel$ | 0 | $-0.96A_\parallel$ $(-1)$ [270 GHz] | $5.01A_\perp$ (4.45) |
| $A_2(2)$ | 0 | $-0.47A_\perp$ | $-0.47A_\perp$ | $5.01A_\perp$ (4.45) | $5.01A_\perp$ (4.45) | 0 [420 GHz] |

lowing only for the interaction between adjacent states requires justification. A calculation of the effective strengths of the axial and transverse dipole hyperfine interactions was undertaken using the crystal-field wave functions of Mujaji *et al.*[2] It was found that there are large transverse dipole hyperfine interactions within the two pairs of $A$ and $E$ states as suggested by the agreement obtained above and the values are in reasonable agreement with the values used in the simple model. In particular, by assuming that the intrinsic axial and transverse dipole hyperfine coupling strengths of the $Ho^{3+}$ ions in the $^5F_5$ multiplet are approximately the same, the predicted ratios of $A'_\parallel/A'_\perp$ agree within 15% for the higher energy pair of states and 10% for the lower energy pair. For the latter pair, the absolute value of $A'_\parallel$ disagrees with experiment by a factor of 1.5. These remaining differences could suggest some inaccuracy in the wave functions used and, indeed, preliminary Zeeman data are at variance ($\sim 10\%$) with that expected from the supplied wave functions.

What is more significant, however, is that a full calculation including coupling between all the four lowest levels of the $^5F_5$ multiplet, remembering to make allowance for larger separations and the smaller coupling coefficients, makes a negligible effect on the spectrum and, therefore, the basis for the very simple model is vindicated. The calculated effective strengths of the dipole hyperfine interaction are shown in Table III. It is also noted that the crystal-field wave functions[2] also support the reversal of the sign of the $g$ value between the adjacent $5F_5$ doublet states as determined by experimental data.

## X. CONCLUSION

In general, for a trigonal $C_{3v}$ center, an $E \rightarrow E$ transition gives $(2I+1)$ axially polarized lines and $(2I+1)$ transverse polarized lines at the sum and difference of the ground-and excited-state hyperfine splittings. In this paper, it is shown that if one of the $E$ states interacts with an $A$ state then, in principle, $(2I-1)$ extra lines in each polarization can be induced via the mixing among the doublet hyperfine levels. However, these $(2I-1)$ extra lines have an asymmetric variation in intensities with the two extra lines closer to the center of the hyperfine pattern being the strongest. If the transverse dipole hyperfine interaction, $A'_\perp$, is larger than the axial dipole hyperfine interaction, $A'_\parallel$, this effect will result in a very distinctive $E \rightarrow E$ hyperfine pattern and a calculation of such a pattern has been illustrated in this paper. The trigonal $Ho^{3+}$ center in $CaF_2$ provides a very clear example where such a strong hyperfine mixing has arisen. In the center, there are two optical transitions where there is a neighboring singlet and doublet interacting through the hyperfine interaction and transitions from the ground doublet to the excited doublet exhibit the predicted pattern of eight almost regular hyperfine lines with two extra lines within the spectrum. The origin of these extra lines is, therefore, clearly established and although there has been no attempt to precisely fit the spectrum, it has been shown that the parameters of a simple model accounting for the major features of the spectrum are consistent with crystal-field analysis of the center.

There have been previous examples of irregularities in the pattern of hyperfine lines but these have arisen from

hyperfine mixing of adjacent states resulting in intensity transfer between adjacent transitions.[9] The present case, however, is an illustration where the hyperfine interaction with an adjacent state has led to a redistribution of the intensity within a single optical transition giving significant strengths to normally forbidden hyperfine transitions.

## ACKNOWLEDGMENTS

We wish to thank M. Mujaji and G. D. Jones for supplying the $CaF_2$:$Ho^{3+}$ crystal and for communicating their polarization and crystal-field fitting results prior to publication. The help of David Wardle in making some preliminary calculations is also acknowledged.

[1]M. B. Seelbinder and J. C. Wright, Phys. Rev. B **20**, 4308 (1979).

[2]M. Mujaji, G. D. Jones, and R. W. G. Syme, Phys. Rev. B **46**, 14 398 (1992).

[3]Z. Hasan, H. Ghafoori Fard, and N. B. Manson, J. Lumin. **45**, 304 (1990).

[4]S. Yatsiv, Physica **28**, 521 (1962).

[5]C. Carboni, R. L. Cone, Z.-P. Han, and M. A. H. McCausland, J. Phys. (Paris) Colloq. **49**, C8-843 (1988).

[6]J. P. D. Martin, N. Rigby, and N. B. Manson (unpublished).

[7]R. M. Macfarlane, R. M. Shelby, and D. P. Burum, Opt. Lett. **6**, 593 (1981); D. P. Burum, R. M. Shelby, and R. M. Macfarlane, Phys. Rev. B **25**, 3009 (1982).

[8]A. Dalgarno, "Stationary Perturbation Theory," in *Quantum Theory,* edited by D. R. Bates (Academic, New York, 1961), Vol. 1, pp. 171–209.

[9]N. I. Agladeze, E. A. Vinogradov, and M. N. Popova, Opt. Spectrosc. (USSR) **61**, 1 (1986).